Università degli Studi di Padova

Dipartimento di Fisica e Astronomia
Galileo Galilei

Corso di Laurea in Fisica

Negative ion beam plasma characterization by retarding field energy analyzer

Caratterizzazione di un fascio di ioni negativi tramite retarding field energy analyzer

Laureando

Filippo Manaigo

Relatore

Dott. Gianluigi Serianni

Correlatore

Dott. Emanuele Sartori

Anno Accademico 2016/2017

Abstract

NIO1 (Negative Ion Optimization 1) is a source of negative hydrogen beams, located at RFX facility in Padua. Its purpose is to analyze the optimal configurations for negative ion beam production and propagation.

The propagation of ion beams in a low-density gas exploits space-charge compensation effects, that consists in the generation and confinement by the beam itself of charged particles that balance the beam charges.

This thesis focuses on the characterization of the beam-generated plasma using a four-gridded probe called RFA (Retarding Field Analyzer) which provides information about compensation parameters.

During this thesis work, the probe was installed and operated in NIO1. These data will be compared with those taken at NIFS, in Toki (Japan) in 2016, to study compensation plasma. These plasma parameters were then compared also with the expected ones, the probe used allowed to estimate compensation plasma parameters succesfully.

Sommario

NIO1 (Negative Ion Optimization 1) è una sorgente di fasci di ioni negativi, che si trova al consorzio RFX, situato a Padova. il suo scopo è quello di investigare circa la configurazione ottimale per la produzione e propagazione di fasci di ioni negativi.

La propagazione di un fascio di ioni, in un gas a bassa densità, sfrutta gli effetti di compensazione di carica spaziale. Questa consiste nella generazione e nel confinamento, ad opera del fascio stesso, di particelle cariche che bilanciano la carica del fascio.

Questa tesi si concentra nella caratterizzazione del plasma generato dal beam tramite una sonda a quattro grigle, chiamata RFA (Retarding Field Analyzer), che fornisce informazioni sui parametri di compensazione.

Durante il lavoro su questa tesi, la sonda è stata installata e ha operato su NIO1. I dati ricavati saranno confrontati con quelli presi nel 2016 al NIFS a Toki (Giappone). Successivamente questi sono stati confrontati anche con i parametri attesi, la sonda usata ha permesso di stimare questi con successo.

Contents

Chapter 1

Introduction

The discovery of two important negative hydrogen ion formation processes (the surface and the volume production) made in the 70s, led to the development of modern negative ion sources. [2]

Nowadays negative ion sources are widely used in various research fields.

They are deployed in high-energy particle physics, as a critical component of particle accelerators.

Ion sources play an important role in fusion research and they are also used in mass spectrometry or for medical purpose.

Thanks to this variety of applications research on ion sources is an essential branch of physics and is important to improve knowledge of phenomena bound to them.

1.1 Beam sources for negative ion beams

High current and high current density ion beam sources are based on a plasma discharge from which ions are extracted. As shown in figure 1.1, beam sources are basically composed by a main body, where plasma is confined and both positive and negative ions are generated. This region is usually kept at high negative voltages to generate negative ion beams.

While plasma is maintained in the main body, some particle flux is lost and gets through, in the simplest case, three grids.

The first one is the plasma grid, in contact with the plasma together with the ion source walls, it is biased at negative potential with respect to the vessel, and this bias voltage normally coincide with the beam energy at full acceleration.

The first grid is followed by the extraction grid, which is also kept at higher voltage compared to plasma grid, but it is still negative respect to the vessel, which is grounded. This voltage is called the extraction potential.

The last grid is grounded and, for this reason, is usually called grounded grid.

As in the example in figure 1.1, a third grid can be placed, which is usually positively biased to prevent the flow of positive ions back into the ion source. This grid is usually called suppressor grid. [6]

In the case of NIO1 the plasma source is kept at a negative potential up to $-60\,\mathrm{kV}$, in contact with the Plasma Grid. Negative ions getting through

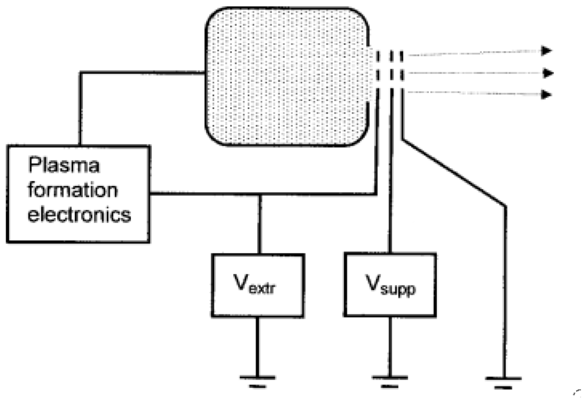

Figure 1.1: A possible negative ion beam source schematics, for example extraction grid could be negatively biased (not as negative as plasma grid, not shown in figure but implicit in che case containing the plasma), and the suppressor can be positively biased

this first grid reach the Extraction Grid, which can reach a maximum negative bias of −54 kV, imposing the electric plasma extraction field, since negative ions after getting through it travel to the grounded grid, which on NIO1 is called Post Acceleration Grid.

In NIO1 there is an additional fourth grid, named Repeller and placed right after the Post Acceleration Grid, which can be positively biased up until 200 V. The repeller prevents positive ions to be accelerated back to the plasma source, that would be damaged otherwise.

Each grid has three rows of three holes, so there are nine independent beamlets composing the negative ion beam. At last NIO1 operates in hydrogen.

1.1.1 Beam parameters

Ion beams are mainly characterized by two parameters:

- The beam energy, i.e. the mean energy per ion in the beam, which depends on the voltage drop between the plasma from which ions are extracted, and the vessel.
- The beam current, i.e. the total current carried by the beam particles, this parameter can be affected by background gas pressure.

As it is well known from the Child-Langmuir law, these two parameters are not independent, an for a given geometry of the accelerating electrodes, the beam current scales as $I \propto V^{3/2}$

After being generated negative ion beams travel through vessel in a background gas, usually kept at low pressure. Collisions between energetic beam ions and gas particles lead to the formation of secondary ions, while the beam energy loss due to these interactions is usually low and can be neglected.

However, there is an issue with beam propagation.

Let's consider the case of a beam entirely composed by ions of the same charge: due to electrical repulsion, in vacuum beam particles would tend to distance themselves, making it impossible for the ion beam to propagate.

1.2 Space charge compensation

In the case of neutral beams for fusion, the precursor ion beams do not travel in a ultra-high vacuum, but in a drift region in which the "tank" pressure is in the range of $(1 - 0.01)$Pa. when travelling through this background gas, secondary charges are generated by collision of the fast beam particles with the gas.

This effect is usually desirable, since secondary ions, having opposite charge respect to the negative beam ions, will arrange themselves into a background sea. Thanks to these "space-charge neutralizing particles" charge density along the path is reduced, so the beam, remaining focused, will propagate straight.

NIO1 in RFX facility is operated in steady-state, meaning that the compensation time is negligible with respect to the lenght of the beam pulse; the ion beam is always transported through a background plasma.

In the peculiar case of negative ion beams for fusion, the beam transport cannot be ensured by magnetic devices, so it must rely on background gas to produce space-charge compensation.

Particles of a charged beam drifting in a vacuum chamber with energy E_0 will collide with a certain cross section σ with residual gas atoms or molecules. As a result of these collisions the gas can be ionized: particles with concordant charge will be repelled by the space-charge potential, while opposite charged particles will get trapped.

A balance between space-charge potential and opposite charged particle temperature (which is related to their thermal speed and tends to distance particles from each other) will be gradually reached, and the beam will lose its tendency to widen.

The necessary time τ to create enough secondary ions for the space-charge compensation can be estimated by: [6]

$$\tau = \frac{1}{\sigma v n_g} \tag{1.1}$$

Let's now consider a H^- beam propagating in a H_2 gas, the same used both at the National Institute for Fusion Science (NIFS) in Japan and in NIO1 (Negative Ion Optimization phase 1) at Consorzio RFX in Padua.

In this situation five different species are to be found: H^-, H^+, H^0 and electrons in a constant desity n_g of H_2 gas. These particles can be generated by the following processes:

$$\begin{aligned}
\mathrm{H}^- + \mathrm{H}_2 &\longrightarrow \mathrm{H}^0 + \mathrm{H}_2 + \mathrm{e}^- && \text{electron stripping} \\
\mathrm{H}^- + \mathrm{H}_2 &\longrightarrow \mathrm{H}^+ + \mathrm{H}_2 + 2\,\mathrm{e}^- && \text{double electron stripping} \\
\mathrm{H}_0 + \mathrm{H}_2 &\longrightarrow \mathrm{H}^+ + \mathrm{H}_2 + \mathrm{e}^- && \text{electron stripping} \\
\mathrm{H}^+ + \mathrm{H}_2 &\longrightarrow \mathrm{H}^0 + \mathrm{H}_2{}^+ && \text{charge exchange}
\end{aligned}$$

Additional ionization processes will occur, caused by the "first generation" electrons which usually have enough energy to generate other electrons by stripping

$$\mathrm{e} + \mathrm{H}_2 \longrightarrow \mathrm{e} + \mathrm{H}_2{}^+ + \mathrm{e} \quad \text{secondary electron stripping}$$

Nominally, NIO1 can accelerate ion beam to a kinetic energy of 60 keV, corresponding to ion initial speed of $v \simeq 0.01\,\mathrm{c}$. Let's consider a typical H_2 gas density $n_g = 1.16 \times 10^{-19}\,\mathrm{m}^{-3}$ and scattering cross section $\sigma \simeq 10^{20}\,\mathrm{m}^2$.

Using formula 1.1, the time needed to compensate for space-charge distribution can be estimated to be:

$$\tau = \frac{1}{10^{20}\,\mathrm{m}^2 * 3 \times 10^6\,\mathrm{m/s} * 10^{-19}\,\mathrm{m}^{-3}} \simeq 3\,\mu\mathrm{s}$$

Space charge compensation evolution was simulated with the same parameters [16] and the results are shown in figure 1.2, where in about 3 µs the beam manages to propagate straight.

For this reason, experimental characterization of the compensation processes and of the secondary plasma parameters is extremely important to optimize the negative ion beam propagation and prevent detrimental effects such as:

- emittance (the radiant flux emitted by a surface per unit area) growth, this effect is visible on the beamlet optics
- beam instabilities due to the presence of stray particles (such as back-streaming positive ions entering the accelerator).

Furthermore, the characterization of the secondary plasma permits a proper interpretation of an important experimental measurement of the beam current, performed by measuring the drain current from the beam dump: beam negative ions and plasma electrons cannot be distinguished in that case.

1.3 Brief RFA description

One of the experimental techniques that can provide the parameters of the compensating plasma consists in measuring the energy distribution of the particles leaving the space-charge compensation region. This can be done for instance by placing a four-grid Rearding field energy analyzer (RFA) in the poximity of the ion beam.

The probe used is composed by four conductive grids, on which a voltage can be imposed, plus a collector, targeted by (depending on the grids potential) positive ions or electrons, where a current signal is measured. All these grids are held inside a cylindrical conductive case, with only the entrance grid exposed to plasma.

Before being collected, ions from the plasma pass through, in order:

1. the entrance grid, which is at the same voltage as the case, it can be either grounded, or left floating
2. plasma electron repeller, a grid with a constant imposed negative voltage, which is used to let only electons reach the collector
3. retarding grid, set to a sweeping potential as needed to repel the ions depending on their energy, whose voltage varies as needed during the acquisition.
4. secondary electron suppressor grid, with an imposed negative voltage, it is used to prevent secondaries electron generated from the other grids to reach the collector and viceversa
5. collector, a plate where the flux of ions arrives, it has the same voltage as the case and it's connected to a circuit, where the current is measured

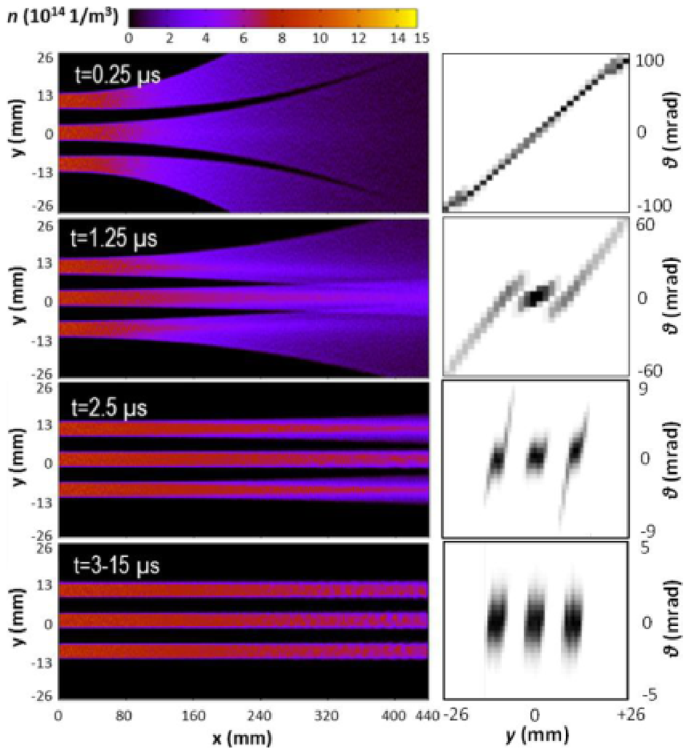

Figure 1.2: on the left-hand side beam shape evolution of three beamlets is shown from above, on the right-hand side is plotted emittance at 410 mm from the reppeller grid on NIO1 [16]

1.4 Thesis purpose

The introduction done so far gives enough tools to write about this thesis purpose, which is to use a Retarding Field Analyzer probe to collect, and later to analyze, data from the compensation plasma around a negative ion beam.

Two cases will be considered: data of 2016 collected at NIFS in Japan, and data collected, during this thesis work period with NIO1, a H^- ion source at RFX facility, in Padua.

The work is divided into the following chapters:

- The first one, an intruduction where physical phenomena, which are the bases of what was studied in the thesis, are explained
- Chapter 2, where a bibliographical research on used RFA structures and configurations is presented
- Chapter 3, where measurements taken at NIFS are analyzed
- Chapter 4, where installation, acquisition and data analysis in NIO1 are described

Chapter 2

RFA probe, review of possible settings

RFA method was first developed to obtain information on the ion distribution function in a plasma discharge.

To get this kind of information a Langmuir probe is not appropriate, because when it is at positive potential, repelling ions, it is also drawing a very high electron-saturation current, which can be much more intense than any current variation due to the plasma ion temperature T_i[9].

A possible solution is to use a "gridded energy analyzer", in which plasma particles can reach the collector only by getting through an electron repeller (a system also known as "gridded Faraday cup"). The simplest gridded probe configuration is shown in figure 2.1, it repels all particle but ions with an energy higher than eV_c, the energy needed to reach the collector biased at potential V_c.

By varying the collector potential V_c it should be possible to obtain the characteristic curve corresponding to the cumulative ion distribution function.

In this thesis work, the objective is to measure compensation plasma with a RFA. This plasma is expected to have its density getting lower the more it get far from the centre

Unluckily, with this kind of configuration, the secondary electrons generated from the grid (which is directly exposed to plasma) are also collected, and these can become dominant, making it difficult to measure ion energy distribution [9].

2.1 Multi-gridded configuration

The probe can be improved by adding more grids, set up in a voltage configuration as the one of figure 2.2.

Furthermore, this voltage configuration allows secondary emitted electrons to be repelled by the grid located between the collector and the retarding grid, which in figure 2.2 is called ion suppressor. Since most of them are generated in the first grids, this configuration effectively prevents electrons from reaching the collector.

The collector potential can either be set at the reference potential of the RFEA box, or negatively biased to ensure a better collection of positive ions.

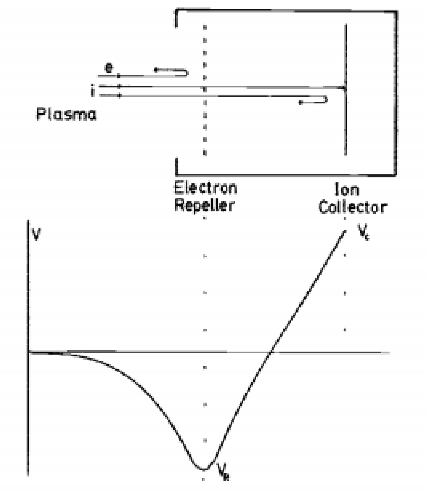

Figure 2.1: Single grid configuration [9]

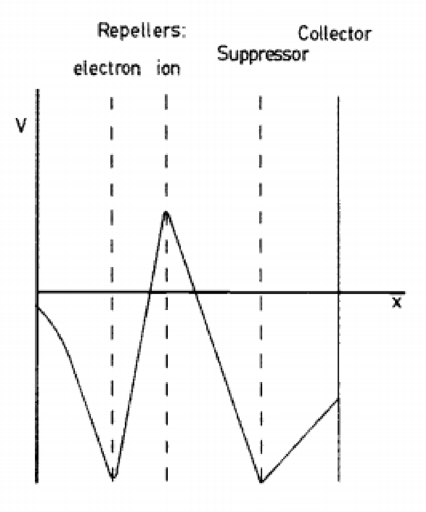

Figure 2.2: Four grid configuration, the ion repeller is actually the floating grid [9]

Moreover, the potential of the retarding grid (sometimes named "discriminator") can vary over time. By sweeping the electric potential it is possible to repel the less energetic ions, thus discriminating the ion population over their kinetic energy. By having a separate retarding electrode, any current that may be generated from the sweeping potential will not affect the measurement.

This kind of probe is suitable in low density plasma where probe dimensions are smaller than Debye length, otherwise an undesired charge density can form in the probe, affecting the measurements. [9]

As a general remark, the external grid (the first of the four grids) shall present a mesh size smaller than the debye length of the plasma facing the probe: this is to avoid plasma screening of the grid itself and plasma entering the energy analyzer. In addition to that, particular care shall be taken to avoid space charge effects inside the analyzer: in that case, the retarding potential could be different than the one imposed at the retarding grid, but be determined by the presence of the ion themselves.

2.2 Alternative voltage settings

What is shown in paragraph 2.1 is just one of the possible voltage configuration for a four gridded RFA.

The four grid analyzers are quite common and were used in the past in many different voltage settings. Even though the voltage settings depend on the purpose of the measurements, on the energy range, the plasma density and other aspects, it is very important to discuss the experiences described in the literature in order to optimize the use of the four-grid analyzer for the purpose of measuring the beam-generated plasma, which in NIO1 case is expected to be at low temperature (not more that 10 eV) and generated at a pressure to the order of magnitude of 10^{-1}Pa

2.2.1 Positive ion distribution measurement

For example figure 2.3 shows a configuration used by M. K. Covo during one of his works [5], where φ_{var} varies from 0 V to 2300 V acting as an energy filter. Collector here is covered with a water based colloidal graphite ("Aquadag") to reduce secondary emission and grounded. This probe has an aperture of 0.8 cm^2 before the first grid, and it is placed at 4 cm from the center of the beam.

Since it was used in high vacuum (5×10^{-7} Torr) with ions with a mean energy of 1 keV and a density of $5.6 \times 10^{-11}\,\mathrm{m}^{-3}$, corresponding to a Debye lenght of 3.1×10^{-1} m it is correct to assume that there is no additional charge density between the grids.

Grid voltages are much higher than the other examples, since M. K. Covo worked with a compensation plasma with 1 keV energy, repeller voltages had to be set accordingly.

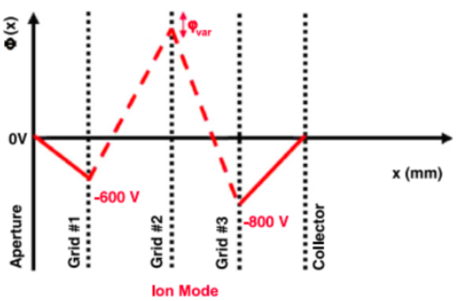

Figure 2.3: RFA grid configuration used by M.K.Covo

Instead C. Böhm, in one of his articles [3] gives an example of a configuration with a highly biased collector, as shown in figure 2.4.

By doing so the ion speed z component between the secondary suppressor and the collector is just sligtly reduced, so there will be less ion loss due to contact with the probe inner case. Also, secondary suppressor, which is still at the lower voltage makes sure that secondaries generated from the collector will not pass through the grid.

Böhm's RFA was designed to work in argon between 0.03 Torr and 0.7 Torr. Its grid are composed by 40 µm wire connected in 150 µm meshes, and grid-to-grid distances are only 1.5 times larger than the mesh size.

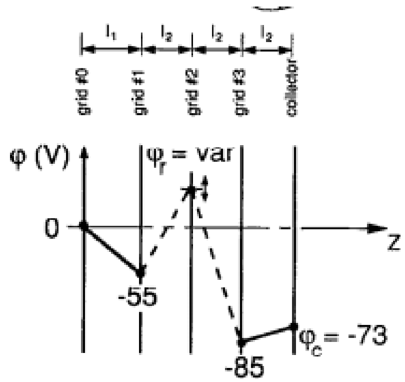

Figure 2.4: RFA grid configuration used by C. Böhm

2.2.2 Electron distribution measurement

RFA probe can also be used to collect electrons and negative ions. To obtain electron energy distribution the configuraton needed is pretty much the opposite of the one used with positive ions: the varying grid must sweep among negative voltages and the filters must repel positive charges.

A possible solution is used by N. Gulbrandsen and Å. Fredriksen in one of their work [8], the configuration used is shown in figure 2.5.

In this configuration the grid, which in ion mode was used as plasma electron repeller, varies among negative voltages, and the grid, which was used as retarding one, acts as ion repeller. The fourth grid, between collector and ion repeller is at a lower voltage than the collector, and thanks to that secondary electrons that would be emitted from the probe collector are suppressed.

This probe was used in argon with a pressure of 0.34 mTorr.

At last, another example is given by M.K.Covo [5], who, in the same conditions he used for his positive ion configuration, set grid voltages according to figure 2.6.

Here particles are initially filtered by an ion repeller, then electrons have to get through the retarding grid, which as usual, according to its voltage φ_{var}, blocks electrons with lower energy.

In this configuration the retarding grid also suppresses secondary electrons, but when φ_{var} is close to zero, the retarding grid does not filter the ones generated at the entrance and at the first grid, affecting the measure.

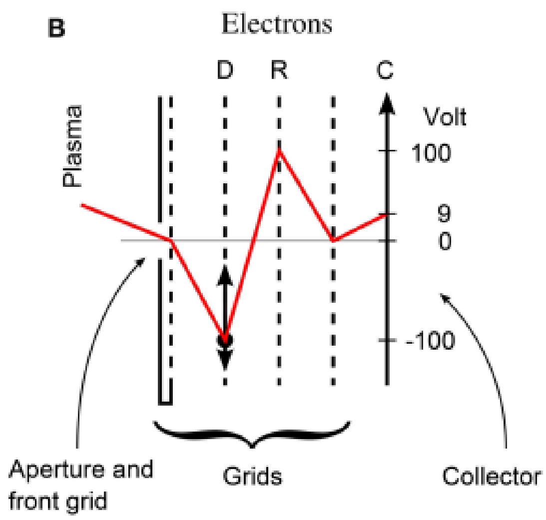

Figure 2.5: RFA grid configuration for electron measurement used by N. Gulbrandsen and Å. Fredriksen

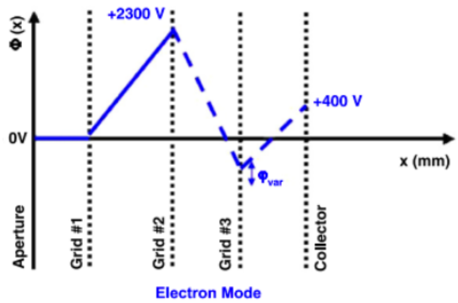

Figure 2.6: RFA grid configuration used by M.K.Covo

2.2.3 Floating case and entrance grid

D. Gaham in one of his works [7] also uses a RFA to measure a radiofrequency-driven plasma with one of the configurations described above, but with one main difference: as shown in figure 2.7 the entrance grid and the RFA case are both at floating potential, a configuration that minimizes perturbation to the plasma.

The collector, which ideally should be isolated from the case thanks to this, is capacitively coupled to the probe surface. So, to prevent any voltage drop, low pass filters are placed between the grids and the electronics.

In this configuration, the external grid and case do not "cut" the ion flux at a certain potential energy, given by their potential. This is because we expect the floating potential to be lower than the plasma potential.

This last hypotesis is true as long as there are negative charged particles with a higher mobility than positive ions, for example if electrons are present in compensation plasma.

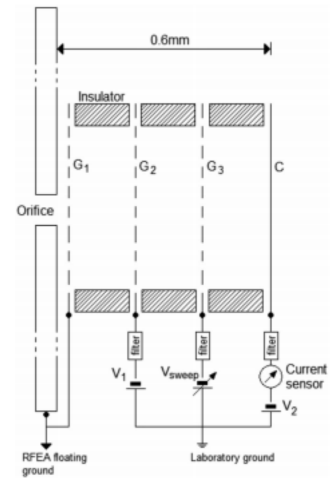

Figure 2.7: RFA configuration used by D. Gahan

2.2.4 Charge neutralisation measurements

During one of his works on H$^-$ ion beams, J. Sherman [17] used an RFA for a purpose similar to the one of this thesis. He used it to measure particles emitted from a H^- ion beam perpendicularly. Figure 2.8 shows the experimental setup.

The configuration used is similar to those described so far, grid-to-grid distance is 5 mm and both suppressor and electron filter have a transparency of 90%, and both retardig grid and the entrance grid, facing the plasma, have a transparency of 70%; this kind of grids are used to minimize electrostatic lens effect, due to equipotential surfaces deformed by grid cavities, that deflects charged particles just as an optical lens deflects light direction.

Moreover, to reduce the effect of the insulating layers adsorbed on grids he kept the whole probe heated at a temperature $T > 350\,^{\circ}\mathrm{C}$. This allows to drastically reduce charged particles deposition on impingement [11].

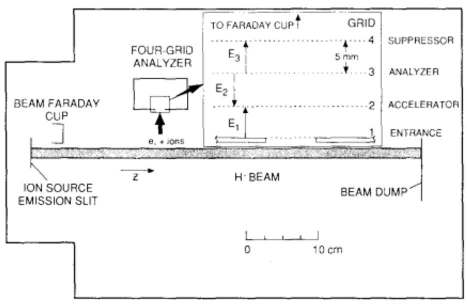

Figure 2.8: RFA configuration used by J. Sherman

He also proposes an interpretation for the measured characteristics. He assumes a constant plasma potential within the beam channel, and outside of it a plasma potential equal to the wall potential.

From the RFA positive ion current cutoff, J. Sherman deducted the beam potential. Plasma temperture was determined by the maximum of the electron energy distribution, shown on the righ-hand side of figure 2.9.

On the left-hand side is shown particle energy distribution of positive ions, the beam potential ϕ_b is given by the retarding grid potential at the ion current cutoff, and the width at the base of the ion energy distribution $\Delta\phi_b$ is the radial potential drop across the beam[17].

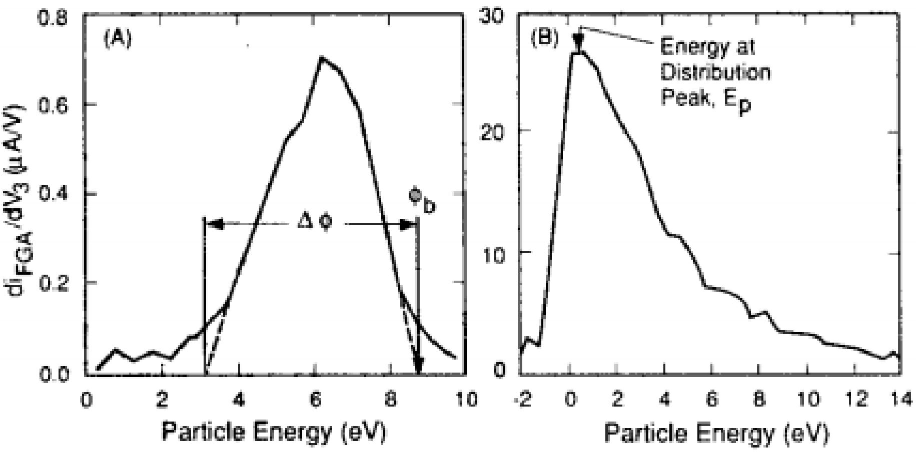

Figure 2.9: energy distributions measured by J. Sherman [17] operating with Xe at a density of $3.5 \times 10^{12}\,\mathrm{cm}^{-3}$

2.3 RFA used at NIFS

In 2016, a four-grid energy analyzer was designed and constructed [13] for measuring the secondary beam plasma in negative ion beams for fusion. The probe was used in the negative ion beam test stand of the National Institute for Fusion Science (NIFS) in Japan[14]. In figure 2.10 schematics are shown.

The entrance grid and RFA case are grounded, the discriminator potential V is swept, the drained current I from collector to ground a measured. This is how the I, V characteristics are obtained.

To effectively filter secondary electrons, the second filter grid is kept at the lowest voltage.

All the grids, the collector, and also RFA case are made of stainless steel (AISI 304L), which can resist to plasma temperatures and polyether ether ketone (PEEK) was used to isolate the conductive steel component of the probe from each other, making sure it will not face plasma.

the RFA case has a diameter of 108 mm, particles get through the entrance grid by a 80 mm diameter opening with rounded edges to minimize electrostatic lens effect.

Due to the low plasma density that is expected, the grid entrance area is very large to maximise the collected currents. Furthermore the grid transparency is quite low, so that the currents reaching the collector are even smaller.

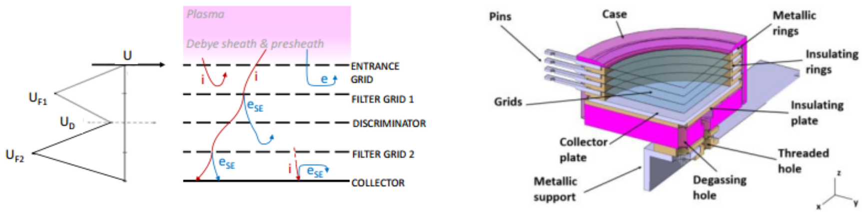

(a) (b)

Figure 2.10: Schematics of the RFA used at NIO1

This RFA has a set of three different kinds of grids, to be used according to plasma temperature and density, whose specifications are summarized in table 2.1. Because plasma must be kept outside of the probe, meshes cannot be larger than one or two times the Debye length. These grids are kept 4 mm from each other.

Meshes per inch	gap width (mm)	wire diameter (µm)	Transparency
14	1.7	0.28	0.74
80	0.207	0.14	0.356
200	0.028	0.028	0.607

Table 2.1: specifics of the sets of grids built for rfx probe, the one actually used during NIO1 measurements is the middle one

2.3.1 Probe electronics

The probe electronics is schematized in figure 2.11. Each grid is connected to the acquisition circuit by a coaxial cable, whose resistance is 0.2 Ω. In the circuit of figure 2.11, all these are schematized with a the resistance R.

Between each pair of grids a parasitic capacitance of 60 pF was measured, while between collector and secondary electron suppressor there are 40 pF, at last there is also another 120 pF capacitance between the collector and the case, which is grounded.

When the ions reach the collector, they generate an input current, which will flow to ground through a shunt R_{out} with a protection (MOV) in parallel, to avoid damage from fast current variations. The MOV however has a non negligible capacitance C_{out} (C_{out} and R_{out} are shown in figure 2.11, their values are respectively 4.1 nF and 5 MΩ). At the extremity of R_{out} voltage V_{out} is measured with a Raspberry Pi [12].

Since parasitic resistances are several orders of magnitude lower than shunt resistance, those are considered negligible. However, the effect of C_{out} is very significant shown in figure 2.12a, so the capacitive term cannot be neglected.

At last I_{in} is to be plotted, so measured V_{out} has to be converted. This can be done simply by dividing it by shunt impedance using equation 2.1.

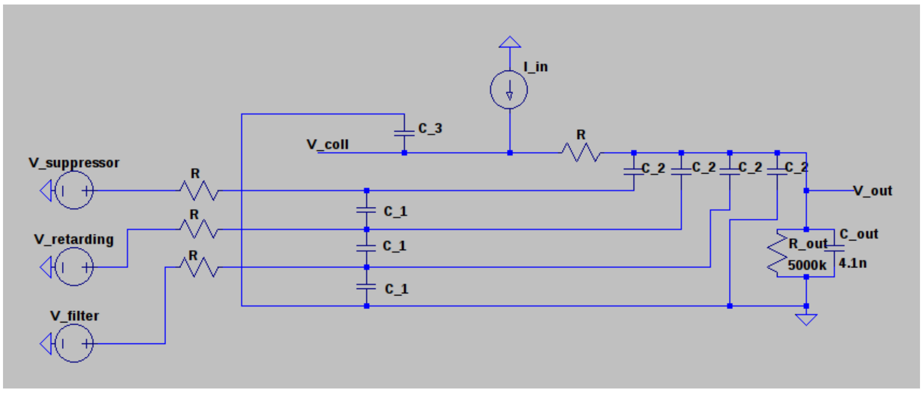

Figure 2.11: RFA electrical circuit

$$I_{in} = \frac{V_{out}}{R_{out}} + C_{out}\frac{dV_{out}}{dt} \tag{2.1}$$

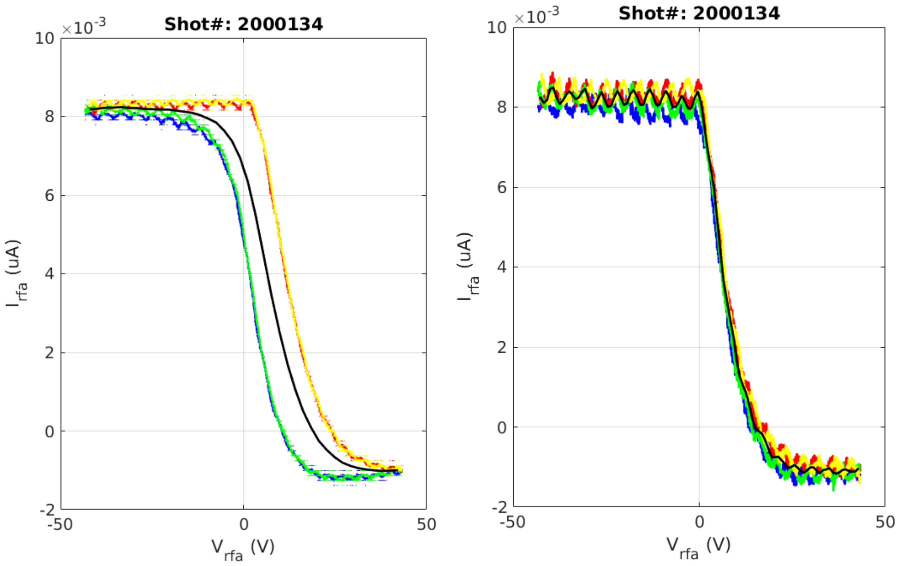

(a) (b)

Figure 2.12: example of current measured as a fucntion of retarding voltage, hysteresis effects are clear on the left-hand side curve; on the right-hand side, I_{in} was calculated including the C_{out} contribution. In this case a flux of positive ions were colleted. As shown, adding signal derivative makes data much more noisy; by smoothing it is possible to get a signal, which is possible to analyze

Chapter 3

Data analysis model and first measurements on NIFS

3.1 Experimental setup

In figure 3.1 NIFS diagnostic and acquisition systems is shown. At the middle-bottom of the photo, under the metal plate there is the drift tube, where ion beam is produced and the RFA probe is located. Immediately on its right-hand side, even if partially hidden, devices for gas injection and the local pumping system for the ion source are visible. On the drift tube left-hand side a thermo-camera is visible. In the upper half of the figure there are the ion source and accelerator.

Figure 3.1: NIFS beam test stand, seen from the top

Inside the drift tube, schematized in figure 3.2, H^- beamlets hit an electrically insulated graphite calorimeter, divided in two independent tiles along the vertical direction, while the RFA probe was used to analyze the perpendicular energy distribution of ions and electrons; finally, a thermocamera allowed to see the beamlet thermal footprint on the grpahite calorimeter during and after the beam pulse. The thermocamera allowed to check shape and intensity of the beamlets.

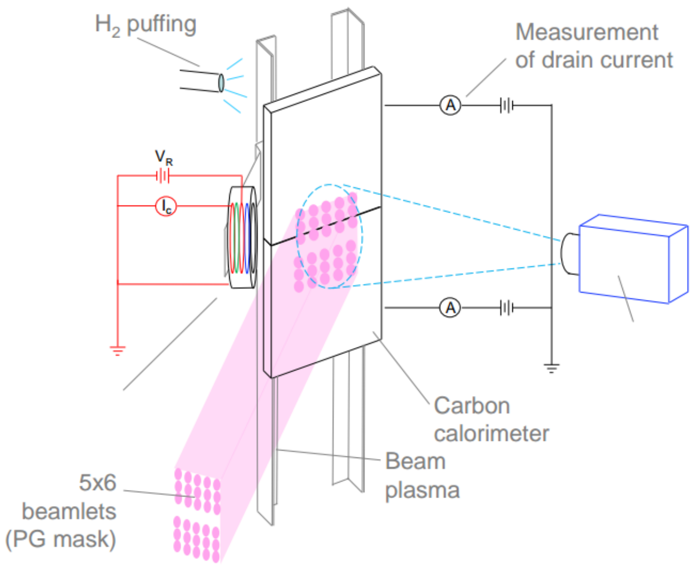

Figure 3.2: beam diagnostic schema

3.2 Data analysis

Data consists in current over voltage characteristic curves, each of them was fitted to obtain parameters of the compensation plasma.

3.2.1 Data fitting model

As said before, the probe was built to be able to analize current collected by the collector as a function of the retarding grid applied voltage. In particular, most of the information is contained between the voltage range that determines a strong variation of the collected current, since current is expected to decrease exponentially as voltage gets higher.

Before being analyzed, data were normalized between 0 and 1 and fitted logarithmically. Normalization was done by using the average values of current in the saturation regions.

To be more specific, the dependence of collected current on variations of the retarding voltage is expected to be described by the equation 3.1.

$$I_{rfa}(V) = min\{1, e^{-\frac{V-V_p}{T}}\} \tag{3.1}$$

Where T is ion (electron) temperature measured in eV, V_p is the plasma potential near the probe, exponential coefficent was imposed equal to 1 to improve fitting precision.

During the process, for positive ion measurement, events that cannot be described by only a decaying exponential, but by two of them, were observed. An example is shown in figure 3.3, due to this fitting model was changed from equation 3.1 to equation 3.2.

$$I_{rfa}(V) = min\{1, e^{-\frac{V-V_p}{T_1}} + A_2 e^{-\frac{V-V_p}{T_2}}\} \tag{3.2}$$

Now two species of ions are considered, A_2 is an unknown parameter to be determined by the fitting because species ratio is unknown.

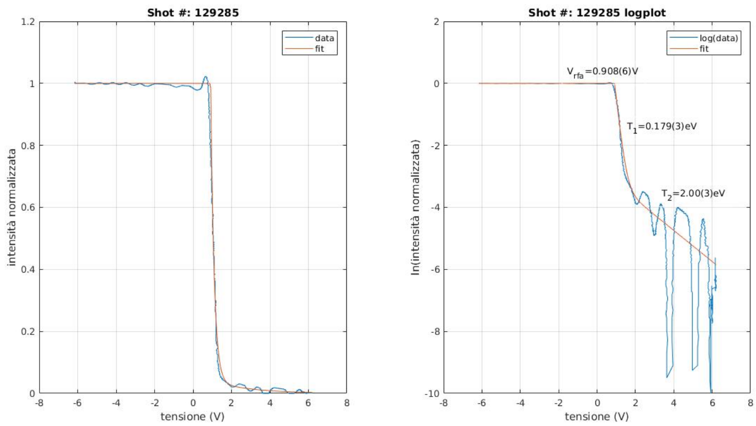

Figure 3.3: An example of double ion temperature, this set of data is taken from a single rampe of shot number 129285, at NIFS.

Fitting model derivation

Data were fitted with equation 3.1. In this section this equation will be obtained and explained.

The RFA basically collects a flux of particles filtered by their energy. Considering a RFA facing the z axis, to get to the collector, charged particles need to have a positive velocity towards z greater than a threshold speed v_0 determined by the probe itself.

This means, translated into equations, that the collected flux is:

$$\Gamma_z = \int_{-\infty}^{+\infty} dv_x \int_{-\infty}^{+\infty} dv_y \int_{v_0}^{+\infty} v_z f(x,y,z) dv_z \tag{3.3}$$

Where $f(x, y, z)$ is Maxwell-Boltzmann distribution:

$$f(x,y,z) = n\left(\frac{m}{2\pi k_b T}\right)^{\frac{3}{2}} exp\left(-\frac{m(v_x^2+v_y^2+v_z^2)}{2k_b T}\right) \tag{3.4}$$

By combining together these two equation, collected flux becomes:

$$\Gamma_z = n\sqrt{\frac{m}{2\pi k_b T}} \int_{v_0}^{+\infty} v_z e^{-\frac{m(v_x^2+v_y^2+v_z^2)}{2k_bT}} dv_z = n\sqrt{\frac{k_bT}{2\pi m}} \left[-e^{-\frac{m(v_x^2+v_y^2+v_z^2)}{2k_bT}}\right]_{v_0}^{+\infty} \tag{3.5}$$

It is possible to substitute particle kinetic energy to particle speed. So integration lower limit becomes the energy that particle needs to reach the collector, which is imposed by RFA retarding grid potential energy, say V.

After calling the constant term A, the equation can be rewritten into:

$$\Gamma_z = Ae^{-\frac{V}{k_bT}} \tag{3.6}$$

Which describes, the collected flux as function of potential energy (therefore of voltage) imposed by the RFA.

However, this voltage is referred to ground, but plasma particles before approaching Debye sheath are at plasma potential V_p. Due to this the equation has to be changed into:

$$\Gamma_z = Ae^{-\frac{V-V_p}{k_bT}} \tag{3.7}$$

That is actually the function introduced in paragraph 3.2.1.

3.2.2 Comparison with plasma parameters

In a pressure scan, the saturation current varies as expected: the presence of denser background gas increase the collision frequency, so more compensation plasma is formed and more ions are collected as shown in figure 3.4.

The trend shown in figure 3.5 is due to the RFA acquisition circuit. Since the collector is connected to ground through a resistance $R = 1\,\mathrm{M\Omega}$, when current is measured, the collector voltage changes accordingly.

In fact, the difference of saturation currents between higher and lower pressure is $\Delta I = 0.2\,\mathrm{\mu A}$, so using Ohm's law, it is possible to know the expected voltage drop.

$$\Delta V = R\Delta I = 0.2\,\mathrm{V}$$

Which is exactly the drop shown in figure 3.5. So this effect can be entirely attributed to collector electronics.

At last, there are no expected correlation between background gas density and measured ionic energy, the graph in figure 3.6 confirm this.

These measures were acquired with grounded calorimeter.

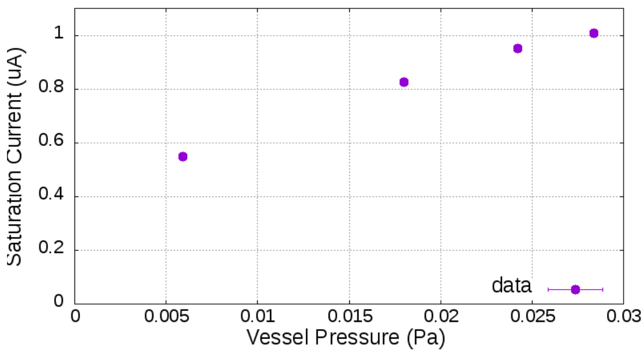

Figure 3.4: saturation current on vessel pressure

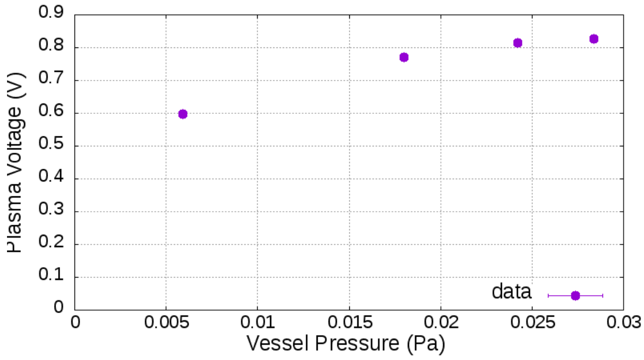

Figure 3.5: plasma voltage on vessel pressure

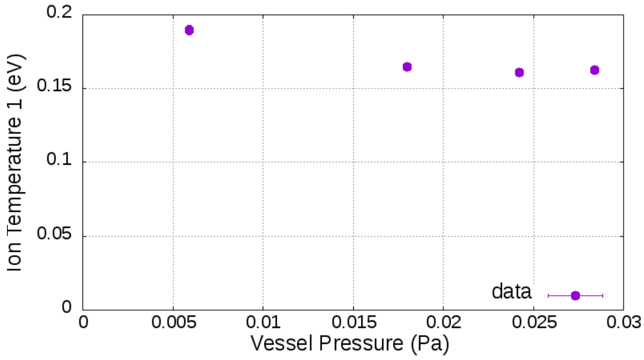

Figure 3.6: ion temperature on vessel pressure

Chapter 4

Probe installation e measurements on NIO1

NIO1 (Negative Ion Optimization 1) [4] is a H^- ion source, located in RFX facility, Padua, which is shown in figure 4.1.

Both source and accelerator are placed at the end of a 2 m chamber (called vessel), which is kept at a desired pressure. Ions are divided into 9 beamlets and before impinging onto a calorimeter are accelerated through three grids.

The nominal beam current is 135 mA at −60 kV, plasma is maintained by a 2 MHz radiofrequency power supply.

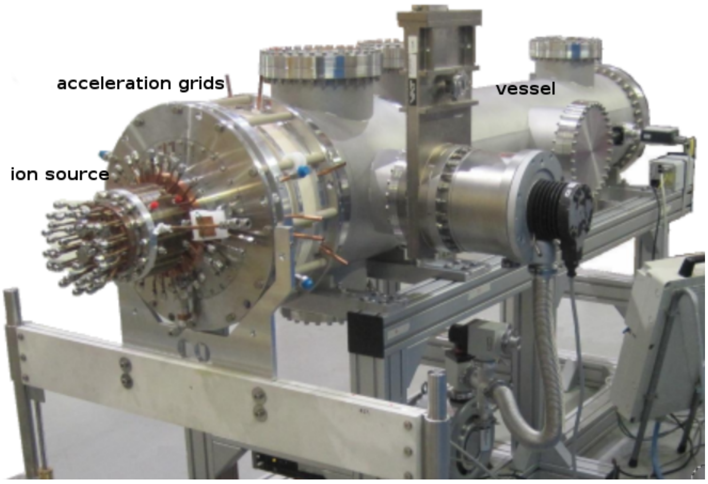

Figure 4.1

4.1 RFA installation

As shown in figure 4.2, during data collection in Japan, described in chapter 3, there was an issue with charged particles depositing on the back of the case, where a small portion of the collector's connector was also exposed.

To avoid this, each grid connector was individually insulated with kapton tape, so the measurments are not affected by particles outside the probe anymore.

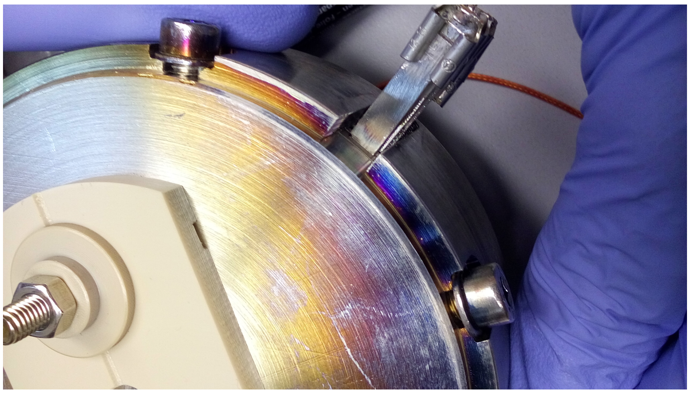

Figure 4.2

On the previous experiments at NIFS, the RFA was placed in a fixed position inside the vacuum chamber. On NIO1 instead, to be able to get data at different distances from the beamlets, the probe was modified to be attached to an endless screw, shown in figure 4.3a. The RFA was meant to be placed over the beamlets, right after the acceleration grids.

To do this, connections between the probe and the external case, placed outside of the chamber had to be modified, in figure 4.3b on the left-hand side this connector is visible. Where each of its pin is connected through coaxial cables to a different probe component, as shown in figure 4.4.

In the boxes placed outside the chamber, are contained Raspberry Pi, which impose all the voltages and read the output voltage (corresponding to V_{out} in figure 2.11), toghether with power supplies and voltage transformers.

4.2 Acquisition process and data analysis

These raspberries, while NIO1 is operating, can be reached by LAN connection, allowing the user to set RFA voltage configuration, start data collection and plot data almost in real time.

The voltage waveform imposed to the retardig grid was triangular, as shown as example in figure 4.5a and a single acquisition lasts about three or four seconds.

From each measurement, current-voltage characteristics are registered, as the one shown in 2.12b, each of them is composed by several voltage ramp.

For each of these ramps, the corresponding characteristic is fitted analogously to what was done for NIFS data in paragraph 3.2.1, with the only difference that in NIO1 data, events with two different ionic species temperatures (characterized by a double exponential trend) were not registered.

An example of the result is shown in figure 4.6

from these fits the following parameter can be extrapolated: saturation current, plasma voltage and ionic temperature. Next step is to analyze the dependence of these parameters on NIO1 source and beam properties.

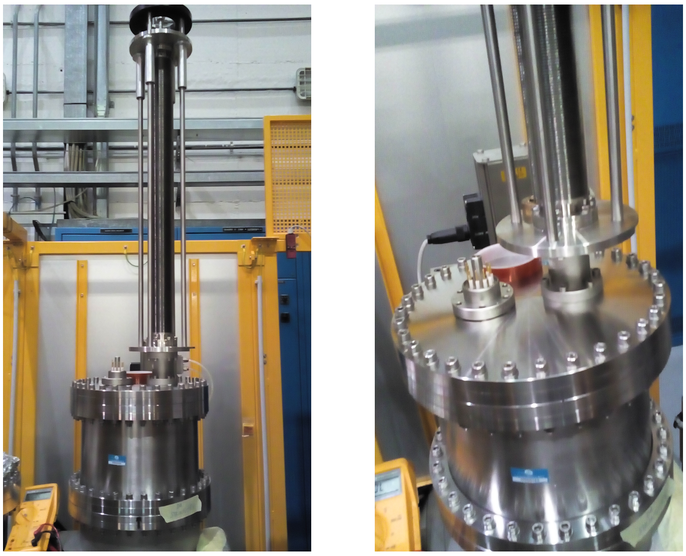

(a) endless screw regulating RFA position

(b) detail of the bottom of the screw, the connectors between RFA and outer cables can be seen

Figure 4.3

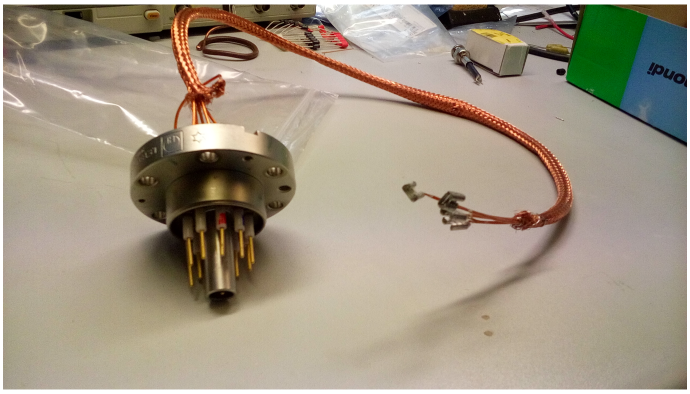

Figure 4.4: rfa connector, also shown in figure 4.3b, five coaxial cables come out from its back, these will be connected to grids and collector. all the cables are protected inside a copper sheath

4.2.1 Radial density profile

To analyze measurements taken while changing the distance between the probe and the beamlets, can be useful to know qualitatively plasma density profile from the beamlets to NIO1 vessel. The profile is expected to depend on species diffusivity. To verify the model effectiveness this parameter will be fitted on data and compared to its expected value.

It is possible to approximate NIO1 to a cylindrical shaped wall, with radius r_{max}, which confines a low density plasma with an unknown density profile. In

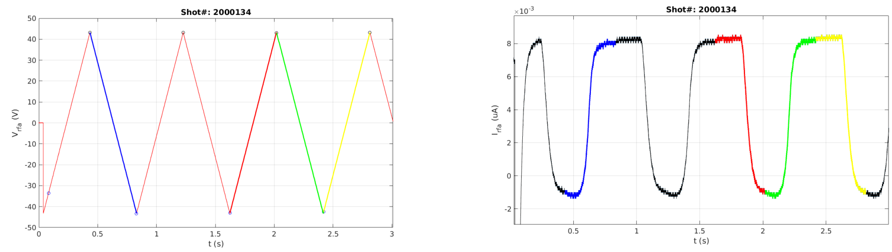

(a) example of an imposed retarding potential

(b) example of a measured current signal

Figure 4.5: in this case time for a sigle ramp to sweep from maximum to minimum potential is 0.4 s

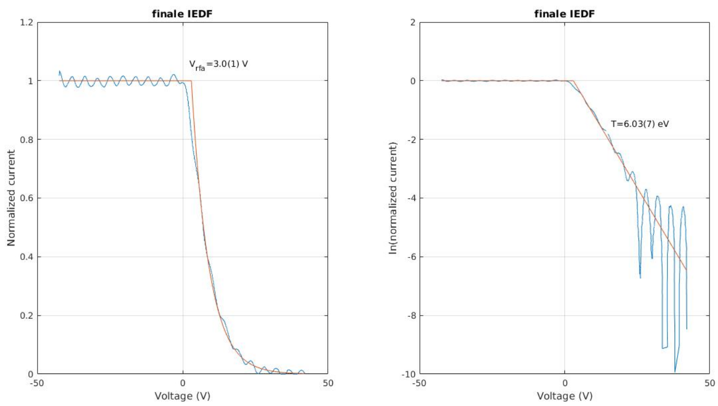

Figure 4.6: Fit corresponding to the yellow characteristic in figure 2.12b, The aquisition was done with the following parameters: vessel pressure 0.432 Pa, extraction grid voltage −2017 V, plasma grid voltage −2220 V, RF power 1100 kW and bias plate voltage 50 V

this region the negative ion beam, with a radius $r_0 \ll r_{max}$, works as a plasma source.

If only a radial density dependency is assumed the problem is reduced to finding a solution for the equation [10].

$$\frac{\partial n(r)}{\partial t} - D\nabla^2 n(r) = -D\nabla^2 n(r) = G_0 \tag{4.1}$$

Whose the first equation is true because we are considering a constant plasma profile, n stands for plasma density, D is plasma diffusivity and G_0 is the source term.

In the considered example, where there's only radial dependency, the equation becomes[10]:

$$\frac{d^2 n}{dr^2} + \frac{1}{r}\frac{dn}{dr} = -\frac{G_0}{D} \tag{4.2}$$

which homogeneous solution is:

$$n(r) = A \ln\left(\frac{r}{R}\right) + B \tag{4.3}$$

Where R is the edge of compensation plasma region, where Debye presheath separates it from the vessel. Since, the RFA is placed outside the beam region, just the region between beamlets and R can be considered.

In this region there is no source term, since secondaries are mainly generated in the beamlets region, so density equation becomes.

$$\frac{d^2n}{dr^2} + \frac{1}{r}\frac{dn}{dr} = 0 \tag{4.4}$$

To define A and B constant in equation 4.3 a boundary condition has to be imposed. The easiest way is to consider particle flux, which has to be constant since in the considered region the is no source term, its value will be obtained in section 4.2.1.

Relation between particle flux and particle density is known in the presheath: [15]

$$n(R) = B = \frac{\Gamma(R)}{c_s} \tag{4.5}$$

where $c_s = \sqrt{\frac{k_b T_e}{m_i}}$ is Bohm velocity, and $n(R)$ was calculated using the general equation 4.3.

The term A is obtainable thanks to Fick's law $\Gamma = -D_a \nabla n$, (where D_a is the ambipolar flux) evaluated in $r = R$.

$$\frac{dn}{dr}(R) = \frac{A}{R} = -\frac{\Gamma(R)}{D_a} \tag{4.6}$$

So radial density profile, outside the beamlets region, is expected to be described by:

$$n(r) = -\frac{R\Gamma(R)}{D_a} \ln\left(\frac{r}{R}\right) + \frac{\Gamma(R)}{c_s} \tag{4.7}$$

To verify the validity of the equation, this plasma profile will be used in 4.2.4, to explain the measurements obtained by changing RFA distance from the beamlets.

From those data diffusivity D will be extrapolated and compared to its expected value, calcolated in section 4.2.1.

At last the vessel radius is $R = 0.2\,\mathrm{m}$.

Flux term

In equation 4.7, particle flux at vessel region $\Gamma(R)$ was used, in the following this term is going to be evaluated in NIO1 case.

The following evaluation is just an approximation, estimated coefficients will be compared to the those obtained by fitting NIO1 data to be sure that the profile assumed is a good approximation. the same will be done for diffusivity which will be evaluated in the next section.

In beam region, energetic H^- with velocity $v = 7.7 \times 10^5\,\mathrm{m/s}$ (corresponding to a $3\,\mathrm{keV}$ beam) and density $n_b = 6 \times 10^{14}\,\mathrm{m^{-3}}$, scatter with the background

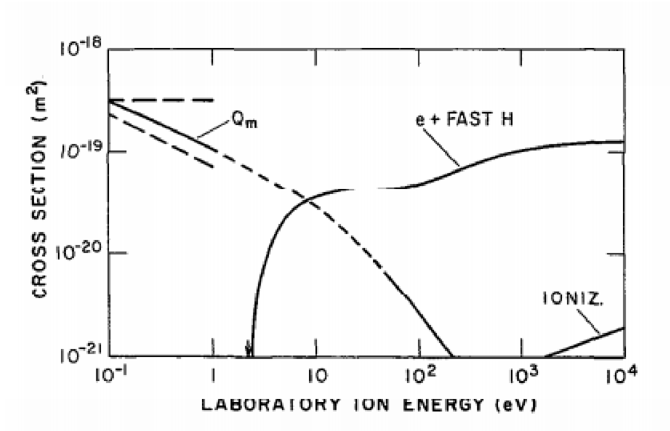

Figure 4.7: H^- on H_2 cross section [18]

gas, composed of H_2 with density $n_g = 4 \times 10^{19}\,\mathrm{m}^{-3}$, this process occur with a cross section σ.

Due to these collisions free electrons and ${H_2}^+$, which forms compensation plasma, are produced. H^- ions suffer a low deflection, so with a good approximation it is possible to assume that they are confined in the beamlets region.

H^- on H_2 scattering cross section are shown in figure 4.7. Now, considering a H^- with 3.5 keV (the same beam energy used in section 4.2.4 measurements), a cross section of $\sigma \simeq 4 \times 10^{-20}\,\mathrm{m}^2$ can be assumed.

By dimensional analysis it is possible to assume that the rateo of particles generated in unit of time and volume, G_0, has the following form

$$G_0 = n_b n_g \sigma v_b \tag{4.8}$$

Source term is limited to the beamlets volume. To evaluate flux at a distance R from the center, after considering an infinitesimal lenght of the beam dz the following equation can be used.

$$\Gamma(R) = \frac{G_0 \pi 9 r_0^2 dz}{2\pi R dz} = \frac{9 I n_g \sigma}{q 2\pi R} \tag{4.9}$$

Where $I = 0.03\,\mathrm{mA}$ and $r_0 = 1\,\mathrm{cm}$ are current and "radius" of a single ion beamlet, since they are nine, the equation above has the multiplication factor of 9.

With these parameters a radial flux $\Gamma(R) 2.4 \times 10^{15}\,\mathrm{m}^{-2}\mathrm{s}^{-1}$ is obtained. Since B from equation 4.3 will be fitted in section 4.2.4, evaluating it can be useful to compare results. Using equation 4.5 $B = 7.7 \times 10^{10}\,\mathrm{m}^{-3}$ is obtained.

Expected diffusivity

The expected ambipolar diffusion value can be estimated by using the following equation

$$D_{amb} = \frac{\mu_i D_e + \mu_e D_i}{\mu_i + \mu_e} \tag{4.10}$$

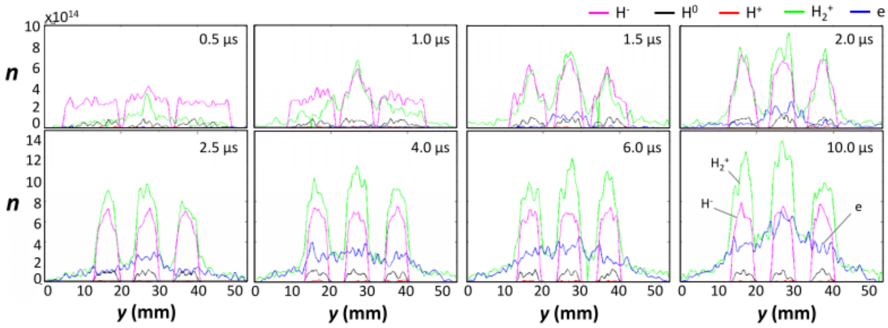

Figure 4.8: Simulation of vertical profile of particles in NIO1 [16], beam density was read from the last graph

where μ and D are respectively the species mobility and diffusivity (i subcript stands for positive ionic species and e for electrons), whose expressions are:

$$\mu = \frac{q}{m\nu}$$

$$D = \frac{k_b T}{m\nu}$$

Where ν is the collision frequency of the charges, which was calculated with the following equation:

$$\nu = n_b \sigma v_b \tag{4.11}$$

Where n_g is background gas velocity, σ is the cross section and v_b is the mean beam particle speed.

μ_e and D_e will be referred to the electrons, while, as shown in figure 4.8, since positive ions in compensation plasma are mainly ${H_2}^+$, μ_i and D_i will be referred to them.

Using the same parameters as in paragraph 4.2.1 and using equations described above, an ambipolar diffusivity of $D \simeq 2.7 \times 10^4\ \mathrm{m^2/s}$ is estimated.

4.2.2 Effect of Acceleration Grid Power Supply

Since in NIO1 grid voltages can be set, it can be interesting to analyze how the beam is affected by changing them and consequently beam properties.

As shown in figure 4.9, NIO1 has two power supplies (excluding the one polarizing the Suppressor grid): the Acceleration Grid Power Supply (AGPS) which imposes the voltage drop between Plasma and Post Acceleration and defines the beam total energy, and the Extraction Grid Power Supply (EGPS), which sets the Extraction Grid potential.

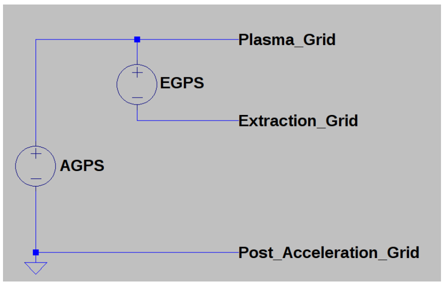

Figure 4.9: NIO1 grids power supply schematics

Current measured by RFA raises as shown in figure 4.10. The current collected with acceleration grid at 4.5 kV is almost two times the one collected when the grid is biased at 2 kV.

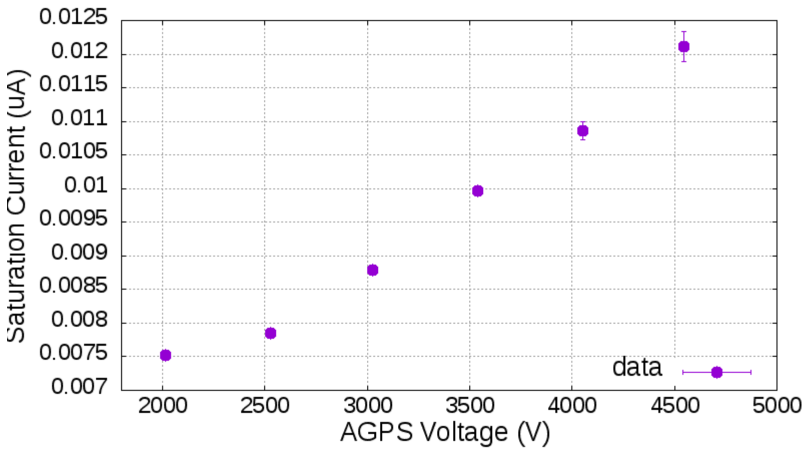

Figure 4.10: saturation current as a function of AGPS voltage

This effect can be explained with cross section: in fact, upon raising the beam energy, the H_2 ionization cross section by beam H^- impact also gets higher.

On the basis of figure 4.11, with grid at 2 kV and at 4.5 kV cross sections of respectively $1.5 \times 10^{-17}\,\mathrm{cm}^2$ and $4 \times 10^{-17}\,\mathrm{cm}^2$ will be assumed.

As seen with equation 4.8, source term G_0 is directly proportional to cross section. Therefore if cross section doubles, compensation plasma density around the beamlets will double too. Thank to this saturation current measured has the trend shown.

To be sure of the dependance just stated, current measured on NIO1 Post Accelation grid (the grounded one) and the carbon calorimeter, that is actually targeted by the beam, as function of acceleration grid voltage was analyzed.

As shown in figure 4.12 during the scan, also the current measured by the Post Acceleration grid doubles. As for compensation plasma this happens because in the grid region ionization occurs, and electrons, with higher mobility, are collected by the grid.

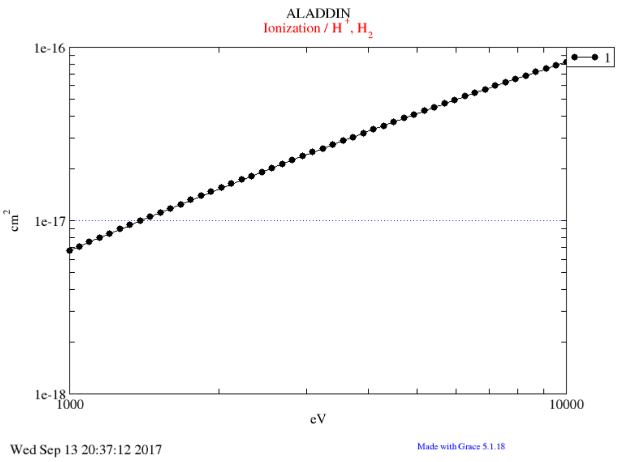

Figure 4.11: H^- and H_2 scattering cross section as function of energy [1]

This is an additional confirmation of the explanation given for figure 4.10 trend.

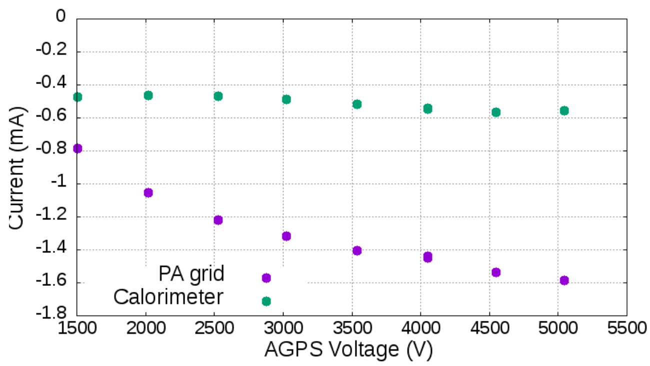

Figure 4.12: measured currents on post accelerator grid and on calorimeter as function of acceleration grid voltage

As said before plasma voltage rises accordingly, its trend could be affected by RFA electronics: the only difference with the example discussed in NIFS data analysis is that now the collector is connected to ground by a resistance of $R = 5\,\mathrm{M}\Omega$.

In figure 4.13 there is a maximum ΔI by $4\,\mathrm{nA}$ which moves collector voltage of $\Delta V = R\Delta I = 20\,\mathrm{mV}$, the effect is much smaller than the $2\,\mathrm{V}$ difference between higher and lower voltage data.

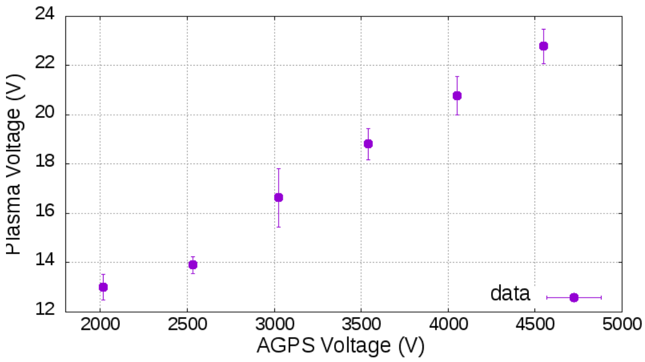

Figure 4.13: plasma voltage as a function of AGPS voltage

At last figure 4.14 shows that compensation plasma temperature is not affected by changing the beam energy.

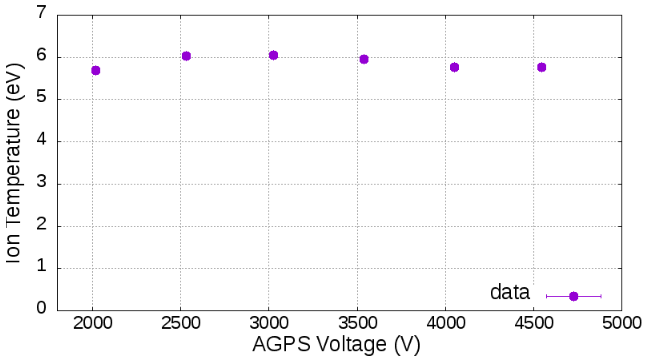

Figure 4.14: ion temperature as a function of AGPS voltage

During this scan electron characteristics were also collected, their temperature as a function of the acceleration grid voltage is shown in figure 4.15, where a linear increase of electron temperature is evident.

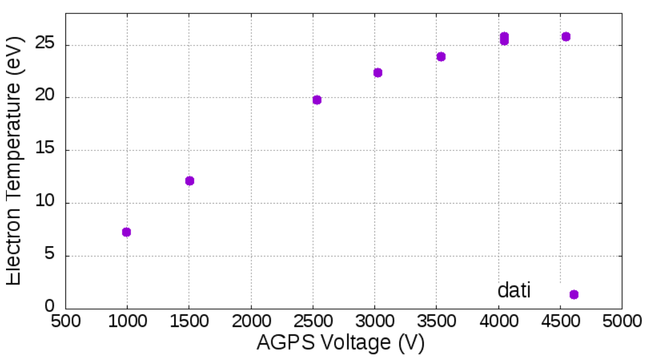

Figure 4.15: electron temperature as a function of AGPS voltage

The scan was made with extraction grid voltage of 500 V (dataset 10983-10993) and a pressure of 0.332 Pa.

4.2.3 Effect of Vessel pressure

Another parameter, interesting to scan, is H_2 gas pressure inside the vessel.

Increasing the vessel pressure increases the rate of production of secondary charges, which is proportional to the gas density, and reduces the mean free path for charge-neutral collisions. Either effects contribute to form a secondary plasma of higher density. This makes the RFA measure a lower saturation current, since there are less particles to collect.

As the current collected by the RFA is proportional to the plasma density, the measurement at a higher vessel pressures shows higher saturation currents as shown in figure 4.16.

As shown in figure 4.17, also plasma potential shows a linear increase similar to the saturation current one.

Indeed with higher pressure more ${H_2}^+$ are generated by collision of background gas with beam particles. ${H_2}^+$ have a low mobility, so they tend to accumulate themselves around the beamlets.

If the gas pressure is such that the confined molecular ions are as dense as the beam, the electric potential becomes flat in the beam region. If the molecular ions become denser than the beam itself, the electric potential of the beam becomes positive; an electron-ion plasma starts to grow. In this regime the beam potential is positive and it is reasonable to assume that the beam potential will grow until an asimptotic solution is reached, in which the beam potential is the potential one can calculate form standard plasma theory.

These measures were acquired with calorimeter biased at 50 V, so they are not directly comparable with the pressure scan studied in in section 3.2.2.

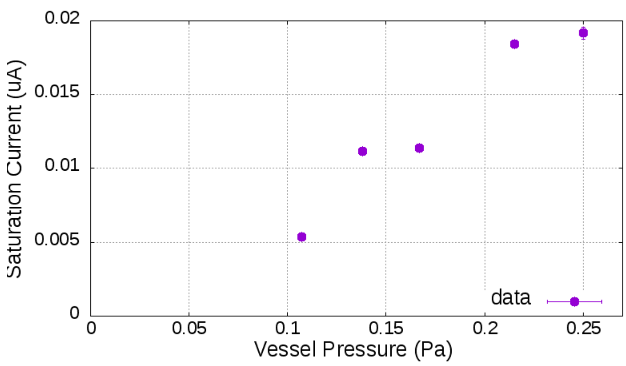

Figure 4.16: saturation current as a function of vessel pressure

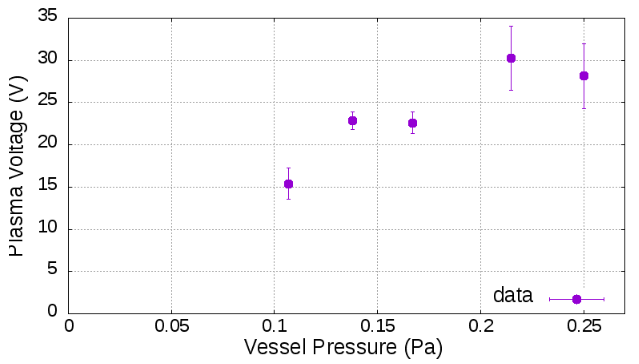

Figure 4.17: plasma voltage as a function of vessel pressure

By analyzing data collected at NIFS in section 3.2.2, for the case of grounded beam dump, no correlation between compensation plasma temperature and background gas pressure was found, the graph shown in figure 4.18 confirms it.

Indeed as said before, scattering with background gas implies an almost negligible loss of energy.

The same trend for electrons is shown in figure 4.19.

And at last, in figure 4.20 an example of fitted ion characteristic is shown.

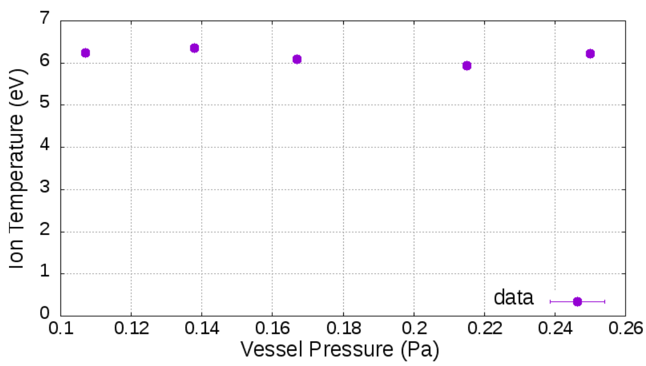

Figure 4.18: ion temperature as a function of vessel pressure

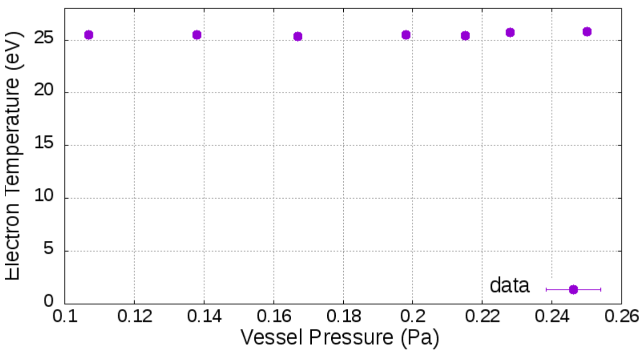

Figure 4.19: electron temperature as a function of vessel pressure

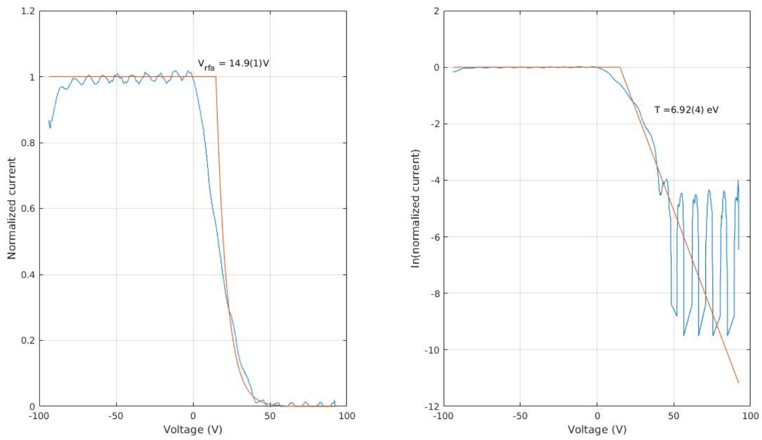

Figure 4.20: Example of a fitted characteristic

The scan was made with acceleration grid voltage of 3.5 kV and extraction grid voltage of 500 V (dataset 11155-11164).

4.2.4 Position scan

As shown in figures 4.21 and 4.22, saturation density shows an evident dependence on position, this was expected since in section 4.2.1 density profiile was calculated, using the same parameters used in this position scan.

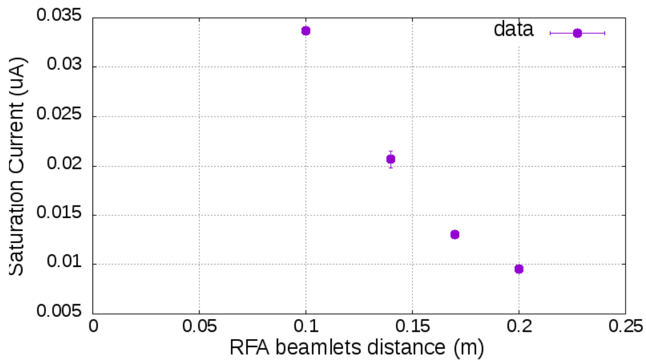

Figure 4.21: saturation current as a function of distance between RFA and beam center

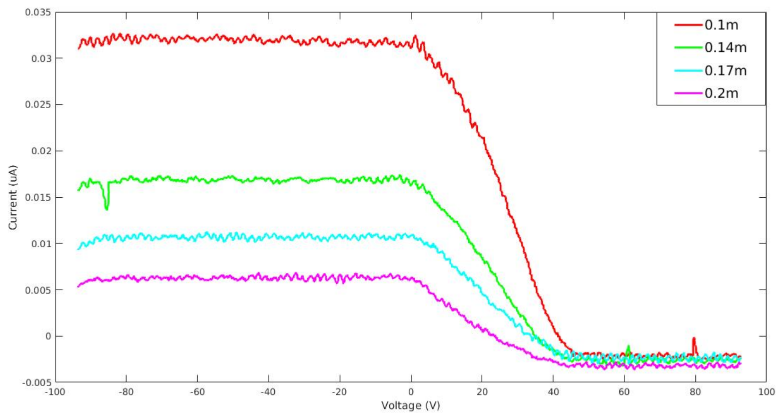

Figure 4.22: Example of measured characteristics during the distance scan

background gas ${H_2}^+$ density is directly proportional to the measured current, in fact:

$$I(r) = \vec{j} \cdot \vec{A}_{coll} = \frac{n(r) e v_{avg} A_{coll}}{4\gamma^4} \tag{4.12}$$

Where $A_{coll} = 1.46 \times 10^{-2}\,\mathrm{m}^2$ is the collector area, $\vec{A}_{coll}$ its normal vector, v_{avg} is the mean speed of ${H_2}^+$ ions with positive velocity component parallel to $\vec{A}_{coll}$, and at last γ is the single grid trasparency, taken from table 2.1.

$$v_{avg} = \sqrt{\frac{8 k_b T_i}{\pi m}} \tag{4.13}$$

$\vec{j}$ and $\vec{A}_{coll}$ are supposed to be parallel, and T_e is electrons temperature.

Thanks to equation 4.12 is possible to plot ${H_2}^+$ density over distance between RFA and beamlets. These points were then fitted with equation 4.3, where A was redefined to explicit the diffusivity term D.

$$n(r) = B - \frac{A}{D} \ln\left(\frac{r}{R}\right) \tag{4.14}$$

(via diffusivity D and constant B), the result is shown in figure 4.23.

Plot result are shown in table 4.1, diffusivity parameter is correct with exception of a factor $4-5$.

So assuming that plasma profile is described by equation 4.7 is a good approximation.

	Fitted	Estimated
A	$2.2(1) \times 10^{10}\,\mathrm{m}^{-3}$	$7.7 \times 10^{10}\,\mathrm{m}^{-3}$
D	$4.6(2) \times 10^{3}\,\mathrm{m}^{2}/\mathrm{s}$	$2.7 \times 10^{4}\,\mathrm{m}^{2}/\mathrm{s}$

Table 4.1: Parameters of figure 4.23 compared with values obtained in section 4.2.1

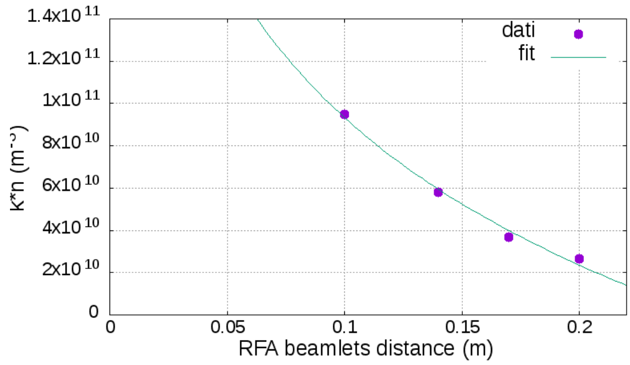

Figure 4.23: kn as a function of distance between RFA and beam center, n does not correspond with ion density, since equation 4.12 is just a rough approximation

In figure 4.24 the voltage trend as function of distance is shown. Since ambipolar diffusion was assumed, a higher voltage in the central region was expected.

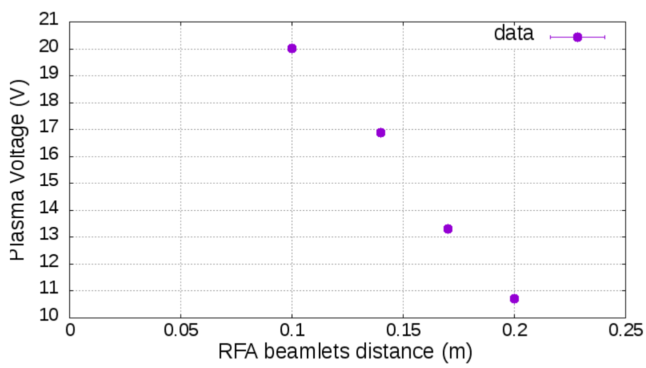

Figure 4.24: Plasma voltage as function as distance between beamlets and RFA

The scan was made with acceleration grid voltage of 3.5 kV and extraction grid voltage of 500 V (dataset 11173-11180) and a pressure of 0.332 Pa.

Chapter 5

Conclusion

This thesis purpose was to analyze compensation plasma, which allows a negative ion beam to propagate straight. A fitting model was obtained and, with that, measured characteristics were analyzed.

Acquired data during pressure scan and acceleration grid voltage scan behave as expected: temperature is independent from both these parameters, while saturation current and plasma voltage increase linearly with these. This is understandable for the reason explained in sections 4.2.2 and 4.2.3.

A scan of the distance between RFA and beamlets was also made. Measured data during this scan shows that voltage decreases getting closer to the vessel and that current decreases logarithmically, according with the obtained density profile.

The RFA is now operative on NIO1. Data collected during this thesis work was difficult to analyze, due to the low current measured, in the best case just a few tens of nA. Grids with larger meshes could improve the measurements in these conditions.

By polarizing the RFA collector it should be possible to use a voltage configuration appropriate for electron measurements.

It could be interesting to implement a floating entrance grid and analyze how the compensation plasma perturbation changes as suggested by D. Gaham, mentioned in section 2.2.3.

Bibliography

[1] *ALLADIN IAEA*. https://www-amdis.iaea.org/ALADDIN/collision.html.

[2] M. Bacal. "Physics aspects of negative ion sources". In: *Nuclear Fusion* 46.6 (2006), S250. URL: `http://stacks.iop.org/0029-5515/46/i=6/a=S05`.

[3] Christian Böhm and Jérôme Perrin. "Retarding-field analyzer for measurements of ion energy distributions and secondary electron emission coefficients in low-pressure radio frequency discharges". In: *Review of Scientific Instruments* 64.1 (1993), pp. 31–44. DOI: `10.1063/1.1144398`. eprint: `http://dx.doi.org/10.1063/1.1144398`. URL: `http://dx.doi.org/10.1063/1.1144398`.

[4] M. Cavenago et al. "Development of a versatile multiaperture negative ion source". In: *Review of Scientific Instruments* 83.2 (2012), 02A707. DOI: `10.1063/1.3670350`. eprint: `http://dx.doi.org/10.1063/1.3670350`. URL: `http://dx.doi.org/10.1063/1.3670350`.

[5] M. Kireeff Covo et al. "Beam interaction measurements with a Retarding Field Analyzer in a high-current high-vacuum positively charged particle accelerator". In: *Nuclear Instruments and Methods in Physics Research Section A: Accelerators, Spectrometers, Detectors and Associated Equipment* 577.1 (2007). Proceedings of the 16th International Symposium on Heavy Ion Inertial Fusion, pp. 139–145. ISSN: 0168-9002. DOI: `http://dx.doi.org/10.1016/j.nima.2007.02.045`. URL: `http://www.sciencedirect.com/science/article/pii/S0168900207003397`.

[6] Brown I.G. (ed.) *The Physics and Technology of Ion Sources*. 2ed. Wiley, 2004. ISBN: 3527404104,9783527404100.

[7] D. Gahan, B. Dolinaj, and M. B. Hopkins. "Retarding field analyzer for ion energy distribution measurements at a radio-frequency biased electrode". In: *Review of Scientific Instruments* 79.3 (2008), p. 033502. DOI: `10.1063/1.2890100`. eprint: `http://dx.doi.org/10.1063/1.2890100`. URL: `http://dx.doi.org/10.1063/1.2890100`.

[8] Njål Gulbrandsen and Åshild Fredriksen. "RFEA Measurements of High-Energy Electrons in a Helicon Plasma Device with Expanding Magnetic Field". In: *Frontiers in Physics* 5 (2017), p. 2. ISSN: 2296-424X. DOI: `10.3389/fphy.2017.00002`. URL: `http://journal.frontiersin.org/article/10.3389/fphy.2017.00002`.

[9] Hutchinson I.H. *Principles of Plasma Diagnostics*. 2ed. CUP, 2005. ISBN: 052167574X,9780521675741.

[10] Allan J. Lichtenberg Michael A. Lieberman. *Principles of Plasma Discharges and Materials Processing.* 2ed. 2005. ISBN: 9780471720010,9780471724254.

[11] K M Poole. "Electrode Contamination in Electron Optical Systems". In: *Proceedings of the Physical Society. Section B* 66.7 (1953), p. 542. URL: http://stacks.iop.org/0370-1301/66/i=7/a=303.

[12] *Raspberry Pi.* https://www.raspberrypi.org/.

[13] E. Sartori et al. "Development of an energy analyzer as diagnostic of beam-generated plasma in negative ion beam systems". In: *AIP Conference Proceedings* 1869.1 (2017), p. 060005. DOI: 10.1063/1.4995792. eprint: http://aip.scitation.org/doi/pdf/10.1063/1.4995792. URL: http://aip.scitation.org/doi/abs/10.1063/1.4995792.

[14] E. Sartori et al. "Experimental campaign at NIFS for measuring beam optics and beam transport Part II - Measurements of beam plasma, RFX-SPIDER-TN-426". In: *Consorzio RFX Tecnical notes* (2016).

[15] E. Sartori et al. "Preliminary studies for a beam-generated plasma neutralizer test in NIO1". In: *AIP Conference Proceedings* 1869.1 (2017), p. 050002. DOI: 10.1063/1.4995783. URL: http://aip.scitation.org/doi/abs/10.1063/1.4995783.

[16] E. Sartori et al. "Simulation of space charge compensation in a multibeamlet negative ion beam". In: *Review of Scientific Instruments* 87.2 (2016), 02B917. DOI: 10.1063/1.4933252. eprint: http://dx.doi.org/10.1063/1.4933252. URL: http://dx.doi.org/10.1063/1.4933252.

[17] Joseph Sherman et al. "H- beam neutralization measurements in a solenoidal beam transport system". In: *AIP Conference Proceedings* 287.1 (1992), pp. 686–694. DOI: 10.1063/1.44814. eprint: http://aip.scitation.org/doi/pdf/10.1063/1.44814. URL: http://aip.scitation.org/doi/abs/10.1063/1.44814.

[18] H. Tawara et al. "Cross Sections and Related Data for Electron Collisions with Hydrogen Molecules and Molecular Ions". In: *Journal of Physical and Chemical Reference Data* 19.3 (1990), pp. 617–636. DOI: 10.1063/1.555856. eprint: http://dx.doi.org/10.1063/1.555856. URL: http://dx.doi.org/10.1063/1.555856.